JOURNAL OF GEOPHYSICAL RESEARCH, VOL. 86, NO. A7, PAGES 5819-5832, JULY 1, 1981

Conjugacy of Electron Microbursts and VLF Chorus

T. J. ROSENBERG, J. C. SIREN, AND D. L. MATTHEWS

Institute for Physical Science and Technology, University of Maryland, College Park, Maryland 20742

K. MARTHINSEN, J. A. HOLTET, AND A. EGELAND

Institute of Physics, University of Oslo, Blindern, Oslo 3, Norway

D. L. CARPENTER AND R. A. HELLIWELL

Radioscience Laboratory, Stanford University, Stanford, California 94305

Information on the location of microburst source regions is limited. One measurement at $L \approx 8.5$ placed the source within 4 R_E of the ionosphere. Measurements at $5 \lesssim L \lesssim 6$, though less conclusive, suggested that source regions may be located either near the equatorial plane or at higher magnetic latitudes along the field line. This paper reports simultaneous observations of bremsstrahlung X rays and VLF radiowave emissions that reveal a detailed correlation between electron microbursts precipitated in one hemisphere and chorus elements of rising frequency recorded at the conjugate point. The measurements were made at Roberval, Canada, and Siple Station, Antarctica ($L \approx 4.1$), during magnetic substorms on July 9 and 15, 1975. The relationship between electron energy ($50 \lesssim E \lesssim 200$ keV) and wave frequency ($2 \lesssim f \lesssim 4$ kHz), and the measured time difference ($0.01 \text{ s} \lesssim \Delta t \lesssim 0.13$ s) between detection of the electrons and waves at ionospheric conjugate points are consistent with near-equatorial cyclotron resonance interactions occurring outside the plasmasphere. In both cases, the observations could be accounted for if a diffusive-equilibrium distribution of electron density along the field line was assumed. The so-called 'collisionless' (or R^{-4}) model of electron density was not in accord with the observations. Some evidence is found for a separation of the wave growth and electron scattering regions. Evidence is also found indicating that the process of electron scattering requires a finite time, up to ~80 ms under the conditions of these observations. The present results suggest that microburst generation regions are located within 20° of the equator on subauroral field lines.

INTRODUCTION

A persistent feature of substorm electron precipitation from the outer radiation zone is the microburst, first described by *Anderson and Milton* [1964]. Microbursts are characterized by durations of ~0.2 s, interburst spacings of ~0.6 s, and small areas (≲100-km dimension) at ionospheric heights. Microbursts are primarily a dayside auroral-zone phenomenon. *Oliven et al.* [1968] found the regions of predominant occurrence to be at $6 \lesssim L \lesssim 8.5$ and magnetic local times $0430 \lesssim \text{MLT} \lesssim 1230$. The occurrence of microbursts at subauroral latitudes and other local times has been reported by *Zhulin et al.* [1973], *Rosenberg et al.* [1977], and *Nakano et al.* [1978]. These and other properties of microburst electron precipitation have been reviewed by *Parks* [1975, 1978].

An important characteristic of microbursts is their close association with the occurrence of VLF chorus, a fact that is taken as evidence that the mechanism of microburst generation involves a wave-particle interaction with VLF chorus. *Oliven and Gurnett* [1968], using satellite observations, found that intervals of electron microbursts only occurred during intervals of VLF chorus emissions. Band-limited chorus, composed primarily of discrete rising frequency elements similar in duration and spacing to microbursts, is the most common form of electromagnetic ELF/VLF radiation observed beyond the plasmapause [*Burtis and Helliwell,* 1969, 1976; *Burton and Holzer,* 1974; *Tsurutani and Smith,* 1977]. The frequency range of chorus, and most other discrete emissions, has been shown to require generation near the equatorial plane [*Burtis and Helliwell,* 1969; *Dunckel and Helliwell,* 1969]. The starting point of most theories of chorus generation is the assumption of wave growth resulting from the Doppler-shifted cyclotron resonance interaction between whistler-mode waves and electrons [*Dowden,* 1962; *Brice,* 1963; *Helliwell,* 1967, 1970; *Helliwell and Crystal,* 1973; *Sudan and Ott,* 1971; *Matsumoto and Kimura,* 1971; *Nunn,* 1971, 1974]. This process is shown schematically in Figure 1. The letters A and B denote separate interactions, either (or perhaps both) of which could take place on a field line at a given time, depending on the conditions relevant to wave growth. The main feature to note is the opposite motions of waves and particles out of the interaction region. *Rosenberg et al.* [1971] and *Foster and Rosenberg* [1976] adopted a similar model to interpret an example of correlated bursts of X rays and discrete VLF emissions. *Helliwell et al.* [1980] employed this model, with allowance for off-equatorial interactions, to explain correlated optical and VLF wave observations. It was shown by *Dowden* [1971], in an extension of *Helliwell* [1967], that under certain conditions the flux of resonant electrons could show spikes resembling microbursts.

Observational evidence of the location and extension along the field line of microburst generation regions is sparse. The rocket measurements of *Lampton* [1967], at $L \approx 8.5$, suggested a source at high magnetic latitude within approximately 4 R_E of the ionosphere at either end of the geomagnetic field line. The measurements of *Anderson and Milton* [1964] and *Haugstad and Pytte* [1977] at $5 \lesssim L \lesssim 6$ were less conclusive on this point and could support generation at any field line location between the equator and the ionosphere.

In this paper we present simultaneous conjugate observations of bremsstrahlung X rays and VLF emissions at $L \approx 4$.

Paper number 1A0467.
0148-0227/81/001A-0467$01.00

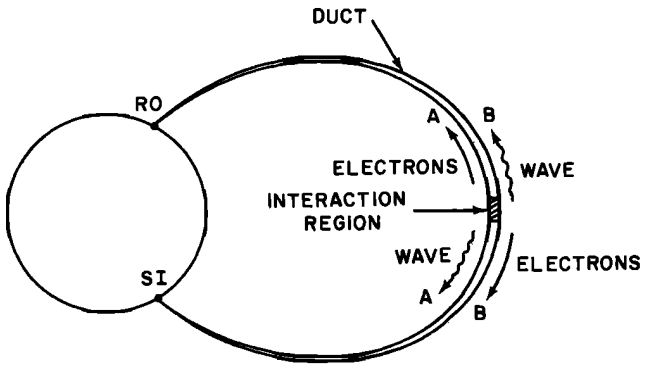

Fig. 1. Schematic model of the Doppler-shifted cyclotron resonance interaction between VLF waves and energetic electrons near the equator. Interactions A and B are identical (though not necessarily independent) except for the senses in which counterstreaming waves and electrons move along the field line.

These observations establish, for the first time, a detailed conjugate correspondence between VLF chorus and electron precipitation microbursts and permit us to examine the location and extent of the interaction region on subauroral field lines. A preliminary account of some of the observations was summarized in *Rosenberg et al.* [1978].

INSTRUMENTATION

Measurements of bremsstrahlung X rays and VLF emissions were made by balloon instruments launched from Roberval, Canada (48.50°N, 72.25°W). Synoptic ground recordings of VLF emissions were also obtained from the conjugate location at Siple Station, Antarctica (75.94°S, 84.25°W). Interhemispheric timing accuracy was maintained to within 10 ms.

Figure 2 shows a sketch of the balloon instrumentation used on July 15, 1975. Digital, multichannel X ray data, analog broadband VLF data, and other information were telemetered to the ground receiving station as indicated. X rays were detected with a sodium iodide scintillation detector with an omnidirectional geometric factor over the upper hemisphere of 476 cm^2 ster. Pulse height energy discrimination with a time resolution of 10 ms was obtained in seven differential channels extending from 25 to 500 keV. The VLF receiving antenna was a one-turn, vertical wire loop contained within a plastic sleeve attached along a circumferential seam of the balloon. With the balloon fully inflated, the cross-sectional area of this antenna is ~300 m^2. The 0- to 5-kHz receiver was bolted directly to the bottom end fitting of the balloon. By placing the VLF receiver on the balloon, interference from power line harmonics and other local noise sources was reduced, and spatial uncertainties were minimized.

On July 9, 1975, a flight was carried out with a balloon instrumented like that shown in Figure 2 but without the VLF experiment. During that flight local VLF data were obtained from the Stanford University broadband VLF receiver at the Roberval site.

OBSERVATIONS AND RESULTS

July 15, 1975

The H components of the magnetic variations at College, Alaska ($L \approx 5.4$), and Roberval are shown in Figure 3 for the interval of interest ($\sum Kp = 24-$). Substorm activity began at ~1030 UT when College was near midnight (LT= UT − 10) and Roberval was near dawn (LT = UT − 5). The maximum intensity at College of ~700 nT (1 nT = 1 γ) occurred at ~1120 UT and was followed by lesser intensifications at ~1200 and 1220 UT. A description of the association of ULF magnetic variations and ionospheric conductivity changes occurring at Siple during this substorm (and during that on July 9, to be discussed below) is given in *Lanzerotti et al.* [1978].

Figure 4 presents electron precipitation data for this period in the form of 1-min averages of the Roberval X ray counting rates (45–65 keV) and the Siple 30-MHz riometer signal. Electron precipitation began at both locations at ~1110 UT (just before the balloon reached its float altitude of 7 g cm^{-2}) and ended by ~1400 UT. During the most intense precipitation, from 1145–1245 UT, the balloon data revealed a complex variety of discrete X ray structures and VLF emissions on several time scales. Qualitative associations similar to those reported previously at this and higher latitudes were evident, but the complexity of the data has made it difficult to establish specific relationships. Our main concern is with a data segment late in the recovery phase of the substorm that contained several groups of multiple X ray microbursts and correlated VLF risers.

X Rays and VLF Emissions at 1300 UT

The main features of the activity at this time, as recorded at Roberval, are shown in Figure 5. The counting rates in two

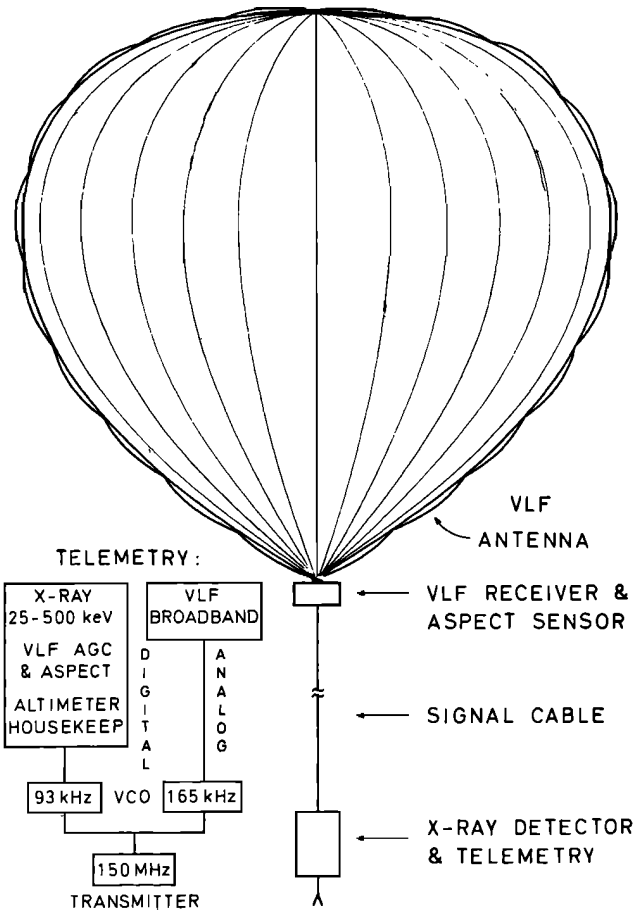

Fig. 2. Balloon instrumentation flown from Roberval, Canada, to detect X rays and VLF emissions. The 0- to 5-kHz receiver is mounted at the bottom of the balloon. Its antenna is a single turn vertical wire loop attached along a circumferential seam of the balloon. When the balloon is fully inflated, the cross-sectional area of the antenna is ~300 m^2 for a balloon of nominal volume 3800 m^3. The X ray detector is a zenith-directed uncollimated sodium iodide scintillation counter.

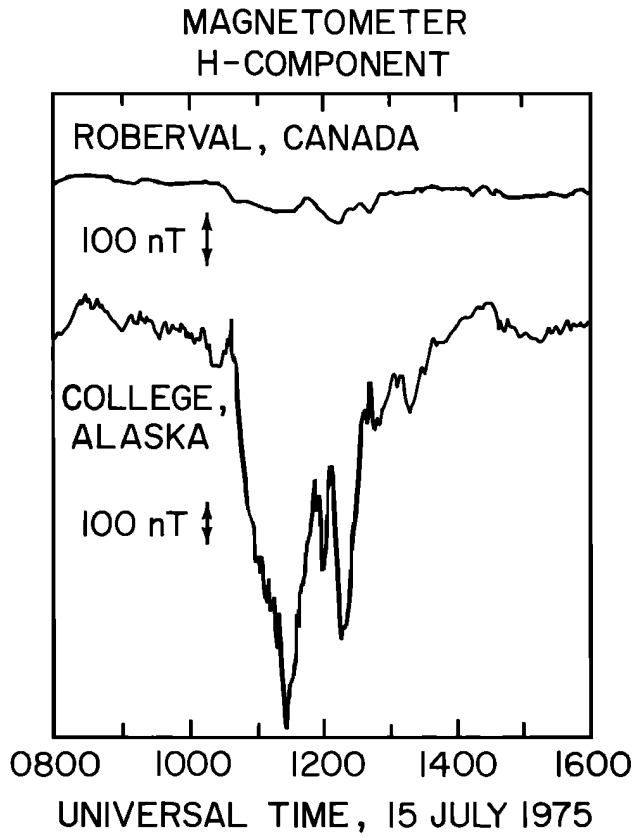

Fig. 3. H-component magnetic variations in the auroral zone (College) and at the subauroral launch site (Roberval), July 15, 1975. During the peak of the substorm activity, College was located near midnight and Roberval near dawn.

different energy channels of the X ray detector are displayed together with a spectrogram of the VLF emissions. This 90-s segment of balloon data contains the most pronounced examples of occurrences of a similar nature lasting from approximately 1255 to 1305 UT. Structured enhancements of the X ray counting rates are closely associated in time with VLF risers in the 2- to 4-kHz frequency range. Counting rate increases occurred also in the 95–125-keV channel, and occasionally in the 125–175-keV channel.

The major burst groups were spaced from 6 to 10 s apart. Statistically significant X ray peaks within the groups had durations of 0.2 to 0.4 s and spacings of 0.3 to 0.8 s, a temporal structure characteristic of electron microbursts. The number of microbursts in each group (typically three to six) generally exceeded the number of distinct risers above 2 kHz (typically one to three). The risers appeared to begin at or near the upper frequency limit of a dense emission band. Many spherics and some whistler segments were also evident in the VLF data at Roberval.

Continuous VLF data were unavailable at Siple Station for the duration of the flight because of VLF transmitter operation. However, the synoptic recording covered a portion of the event from just after 1300 UT and made it possible to study the conjugate aspects of one of the burst groups in detail. Figure 6 shows the conjugate VLF recordings for the section from 1300:06 to 1300:12 UT. The corresponding 45–65-keV X ray count rate is also shown. It is interesting to note that the dense band of emission activity below ~2 kHz at Roberval was largely absent at Siple, whereas the dense hiss band observed at Siple, above ~2 kHz was absent at Roberval. Thus, there was considerable asymmetry in the characteristics of the 'background' emission activity at this time at these two nominally conjugate locations.

More to the point, however, at Siple there is embedded in the hiss band a sequence of risers spaced~0.5 s apart, approximately equal in number to the number of X ray microbursts in the Roberval group. The first tone in the sequence occurs at ~6.5 s and the last tone at ~11 s. These emissions seem first to have ascending and then descending upper and lower cutoff frequencies, with the highest frequencies being reached in the interval from 7.5 to 8 s. At Roberval, only two distinct tones are evident in the same frequency range: at ≅7.8 and ≅8.5 s. Note further that the slopes df/dt of the rising tones are the same at the two locations. If the individual elements had been simple echoes of a single wave packet, these slopes would have been measurably different at the conjugate locations because of whistler dispersion. Therefore, the individual ele-

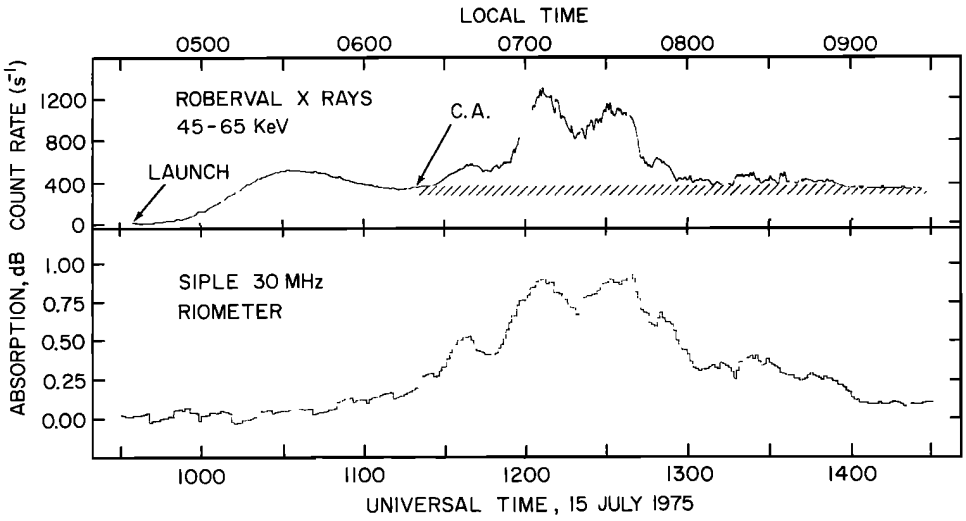

Fig. 4. Substorm electron precipitation at conjugate points of the $L = 4.1$ field line, July 15, 1975. (top) Counting rates in the Roberval 45–65-keV X ray channel and an estimate of the cosmic ray background level. The balloon was launched at 0926 UT and reached a stable ceiling altitude of 7 g cm^{-2} at 1120 UT. (bottom) Relative ionospheric absorption recorded by the Siple 30-MHz riometer.

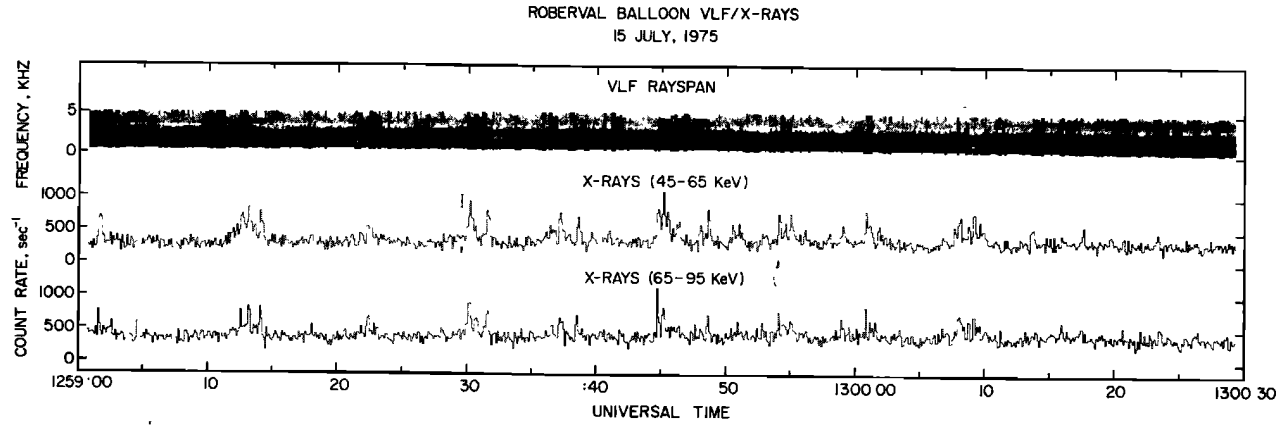

Fig. 5. A 90-s segment of simultaneous balloon recordings of VLF spectrum from 0 to 5 kHz and X ray counting rates in two differential energy channels. A gray scale technique is used to display the VLF spectra, with relatively more intense signals shown darker. The X ray data are plotted in 0.1-s averages.

ments cannot be simple echoes of a single wave packet, but represent separate interactions.

Cross-Correlation Analysis

The data presented in Figures 5 and 6 suggest that the X ray microbursts observed at Roberval were more closely associated with the sequence of risers observed at Siple than with the few risers observed at Roberval in the same time interval and frequency range. To examine this point further, the VLF signal was bandpass filtered in the 2–4-kHz frequency range, and detected, digitized, and cross-correlated with the X ray data in 0.1-s lags. The digitized data sets used in the computation are shown in Figure 7. Beneath each of the VLF data sets short bars show the times from lower to upper cutoff frequency of riser elements that stand out in the spectrograms of Figure 6.

The results of the cross-correlation analyses confirmed the impressions found from the visual comparisons of the recordings. We show the results for the 45–65-keV X ray channel in Figure 8. The highest correlation coefficient is obtained between the Roberval X ray microbursts and the 2–4-kHz Siple risers, with the X ray bursts lagging by 0.1 s. This peak value is 3.5σ above random correlation. Taking account of the filter response, and scaling and timing uncertainties, we estimate that the centroid of the actual correlation peak is at 0.07 ± 0.06 s. Similar results (not shown) were obtained with the 65–95-keV X ray data. It is of interest to note that the Roberval VLF results show no significant correlation with the Roberval 45–65-keV X ray counting rates at this time resolution, despite the obvious association of chorus and X ray bursts shown in Figure 5.

July 9, 1975

The H components of the magnetic variations at College, Alaska, and Lac Rebours, Canada (47.87°N, 72.45°W), are shown in Figure 9 for the interval of interest ($\sum Kp = 31$ this UT date). The Lac Rebours H variations are shown because the Roberval magnetometer went off scale for several hours. Substorm activity began at ~0820 UT when College was in the premidnight sector and Lac Rebours was in the predawn sector. The maximum intensity at College of 1100 nT occurred at 0945 UT. The magnetic field at both College and Lac Rebours recovered steadily to undisturbed levels after this time. In Figure 10 are shown Roberval 45–65-keV X ray counting rates and Siple 30-MHz absorption in the same format as Figure 4. Electron precipitation began at Siple at 0900 UT and was detected by the ascending balloon at Roberval as early as 0930 UT. Precipitation ceased at both sites at ~1130–1200 UT.

Our concern here is with an interval late in the recovery phase, during which many groups of multiple X ray microbursts and correlated VLF risers occurred. An interval of a highly significant correlation between groups of electron microbursts at Roberval and pulses of 30-MHz absorption at Siple occurred during the main phase of the event and has been reported elsewhere [*Siren et al.*, 1980]. The absence of a significant correlation between X rays and the weak VLF chorus observed at the conjugate point during the main phase may be attributed in part to the (hypothesized) absence of local field-aligned ducts of enhanced ionization and to the high level of *D* region absorption (4 dB) at that time.

X Rays and VLF Emissions Between 1045 and 1155 UT

Broadband VLF recordings were made 1 min in each 5 min at Siple, and continuously after 1059 UT at Roberval. Between 1045 UT, when significant 2–4.5-kHz VLF emission activity began, and 1155 UT, when the X ray fluxes fell to near-background levels, correlations of various levels of significance occurred between Roberval X ray fluxes and VLF emissions at both Roberval and Siple. In contrast to the July 15 event, the VLF emissions at Roberval and Siple had many similar characteristics and were often found to be correlated in detail, with a measurable lag, as in Figure 11. The most significant correlation, however, was found between the Roberval X ray fluxes and the Siple VLF emissions in the interval 1100–1125 UT. During this time, microbursts and chorus were occurring almost continually at the respective conjugate points.

An example of such an association is shown in Figure 12. The 0–5-kHz VLF spectrum contains an intense but relatively featureless band of noise below 1.8 kHz and a band of chorus risers between 2 and 3.5 kHz. Closely associated with most of the riser elements is an individual X ray microburst observed at Roberval. The association is much like that shown in Figure 6 for the July 15 event. Also given in Figure 12, to the same time scale, is a plot of the relative 2–3-kHz VLF-integrated signal amplitude. This shows a good correlation between the amplitude of the microbursts and the associated riser ele-

ments. It was mentioned above that VLF emissions at Roberval were often correlated in detail with those at Siple, with a distinct lag. A careful comparison of Figures 11 and 12 will reveal that those chorus risers at Siple that have counterparts at Roberval are also the ones that are associated with microbursts at Roberval. This fact aided greatly in the analysis to be presented below. It should be mentioned that the slopes df/dt of the risers at Roberval and Siple are not significantly different, even though whistler-mode propagation (and consequent frequency-dependent dispersion) played a part in connecting the conjugate phenomena.

Cross-Correlation Analysis

Cross correlations were carried out between the Siple 2–3-kHz VLF integrated signal amplitude and the X ray counting rates in various energy channels. We present here the results from the 45–65-keV X ray data, which has the best statistics. Significant correlations were also found in all other energy channels between 25 and 175 keV. X rays above 175 keV did not deviate significantly from background levels and were uncorrelated with VLF emissions. As was done for the July 15 data, the correlations were computed using 0.1-s averages. The principal differences with the July 15 analysis are that several independent parallel data sequences were available, at 5-min intervals, and the sequences were much longer (>50 s).

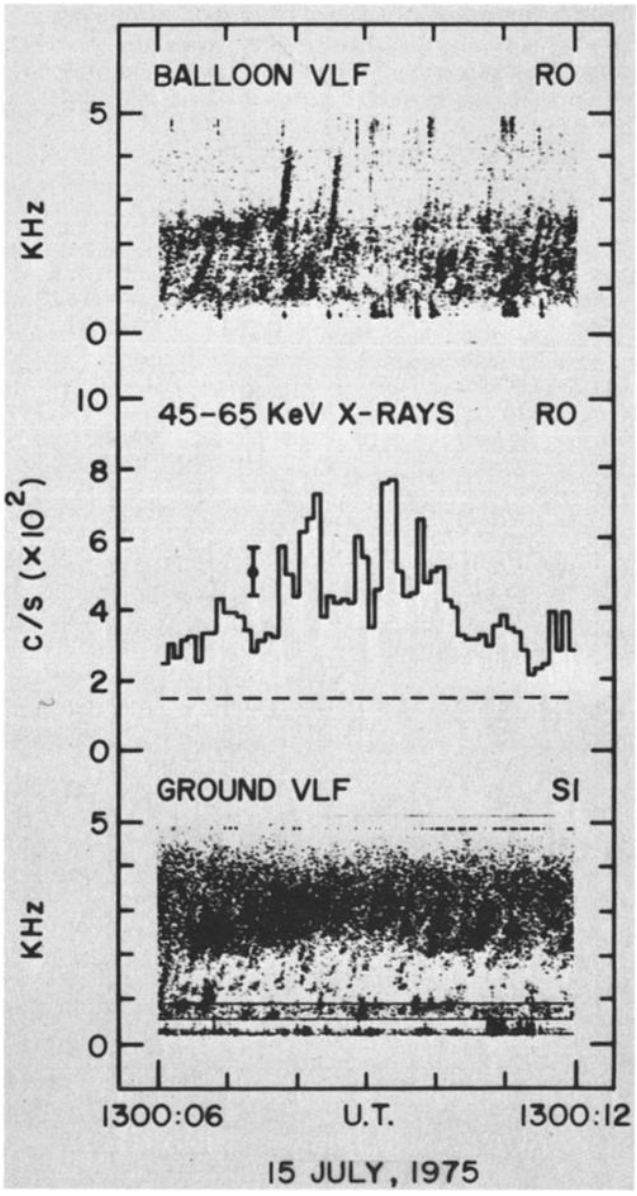

Fig. 6. VLF emissions recorded at conjugate points of the $L = 4.1$ field line and 45–65-keV X ray counting rates at Roberval during one of the burst groups shown in Figure 5.

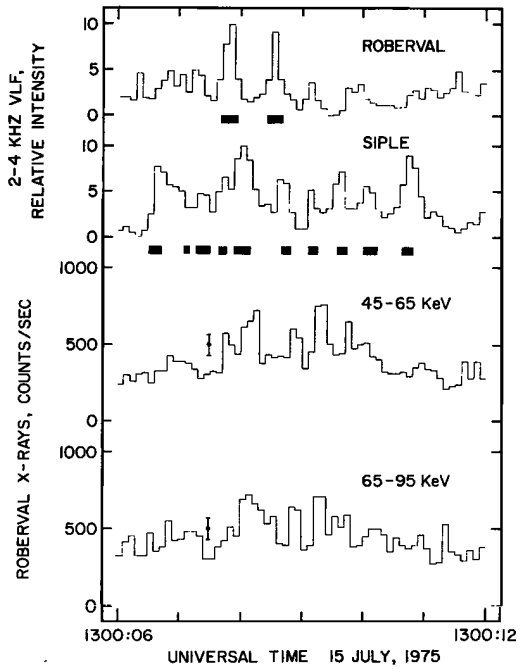

Fig. 7. Relative VLF intensity at 2–4 kHz for the spectra of Figure 6 and the associated X ray counting rates for two energy channels. Short bars beneath each of the 2–4-kHz data sets depict the duration from leading to trailing edge of the pronounced riser elements in the VLF spectra.

The cross-correlation computation for 1110 UT is shown in Figure 13. The similarity of the prominent central peak to that in the July 15 cross correlation (Figure 8) is evident, indicating a comparable relationship between the precipitation microbursts and the chorus risers. Because of the length of the data sequence the centroid of the cross-correlation peak could be calculated to much greater precision (a small fraction of one lag) than for the July 15 data. For this particular 51-s interval the centroid was at 0.057 ± 0.020 s.

Cross correlations were also computed for 1100, 1115, 1120, and 1125 UT. In each case a maximum correlation coefficient of 0.50 or greater was found. The calculated cross correlation centroids are shown in the bottom panel of Figure 14. With the possible exception of the 1125 UT centroid, the correlations show no consistent trend with time.

The lengths of the data sequences also allowed the peak widths (of the cross-correlation peak and also of the X ray and VLF data autocorrelations) to be calculated and compared with high precision. (If the particle-related peak widths were measurably longer than the wave-related peak widths, it might indicate that the process of scattering took place over an unexpectedly long portion of the magnetic field line. Or, if the cross correlation peaks were broad, it might indicate, for example, that some unspecified intermediate process(es) with finite time constants was acting on the generated wave packet before the main scattering commenced.) The peak widths as given by the full width at half-maximum (FWHM) measure

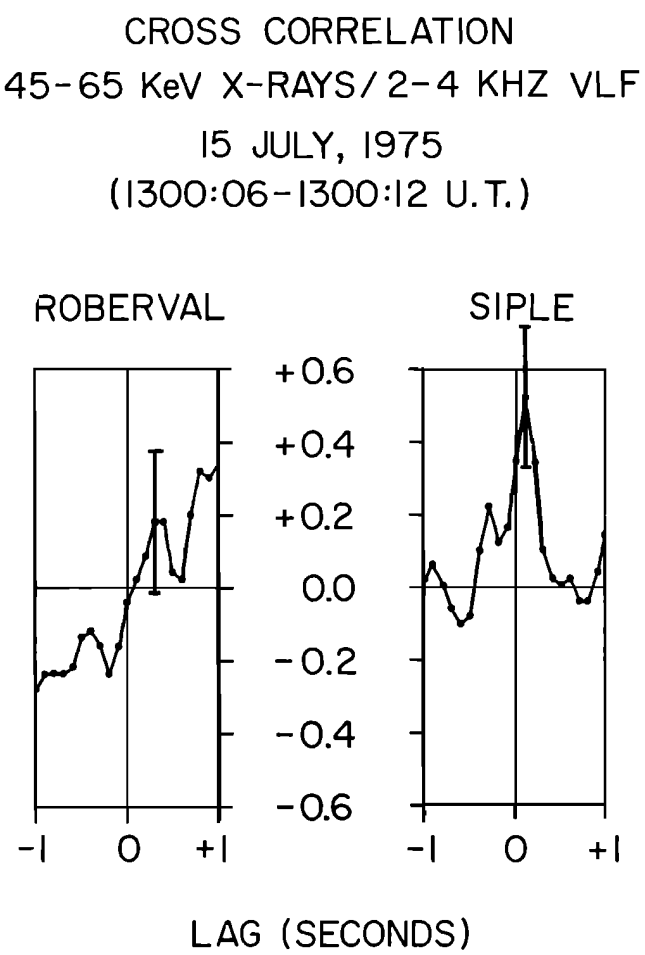

Fig. 8. Cross-correlation of the VLF data sets of Figure 7 with the X ray counting rates in the 45–65-keV channel in lags of 0.1 s. The calculations are meaningful only for lags up to ± 1.0 s (83% of the data). The most significant result is the positive correlation between the Roberval X rays and the Siple risers (right-hand plot), with the X rays delayed by 0.1 s. Error bars indicate ± 1 standard deviation.

are shown in the middle panel of Figure 14. Although the cross- and auto-correlation peak widths vary over time, evidently they do so together, and (except for 1125 UT) in each case the peak width values are so similar that they are consistent with all being identical. Unlike the earlier data intervals, the 1125 interval included intense whistlers. Some of these triggered the strongest chorus bursts during the interval. These whistlers probably broadened the VLF autocorrelation and the cross correlation and may have shifted the cross correlation centroid as well. Consequently, the correlation results at 1125 should not be regarded as significantly different from the 1100–1120 UT results.

Equatorial Electron Density

The propagation time of whistlers can provide a fairly precise means of determining the magnetospheric electron density along the ray path of propagation. Unfortunately, whistlers were few during the correlation event. Good propagation-time data were available in the conjugate chorus riser elements themselves. As was mentioned above, many of the chorus risers were observed first at one site, then at the conjugate point. A more complex process than simple echoing was taking place, since the "echoes," as mentioned above, did not show the additional dispersion one would expect from whistler-mode propagation. The process of reemission or retriggering was occurring as the wave packets traveled from Siple to Roberval. Reemission sometimes requires a finite time less than ≈0.1 s [*Helliwell*, 1965, p. 235]. However, the large slopes df/dt of the risers at both sites in this event are evidence that the process of retriggering took very little time. This is consistent with the near-equality of cross- and autocorrelation peak widths mentioned above. We have ignored retriggering in estimating the wave travel times.

Travel times were estimated by overlaying the VLF spectra (such as in Figure 11) from the conjugate points and sliding one in relation to the other in order to find the best overall match for each common interval. The precision of this method is at least 0.15 s, and on the better data is 0.10 s. Travel times measured by this method are shown in the top panel of Figure 14. (At 1100 UT the chorus riser elements occurred first at Roberval, then at Siple. After 1110, the reverse was true. No case was found of northward and southward interhemispheric propagation both occurring in the same 1-min record.) Travel time estimates of ≅0.68–≅0.95 s were obtained by this method. One scalable whistler occurred at 1115 UT, propagating near or on the local L shell. The wave travel time at 2.5 kHz was $0.7^{+0.10}_{-0.05}$ s, in good agreement with the

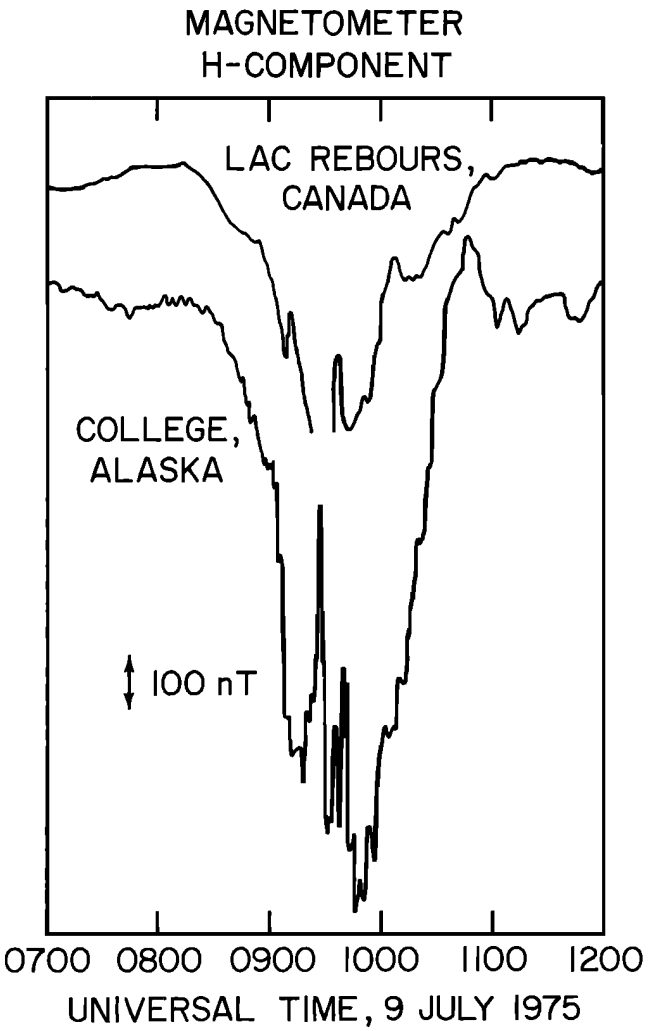

Fig. 9. H-component magnetic variations at College, Alaska, and at Lac Rebours, Canada, near Roberval, July 9, 1975. As for the July 15, 1975 event, during the peak of the substorm activity, College was near midnight and Roberval near dawn.

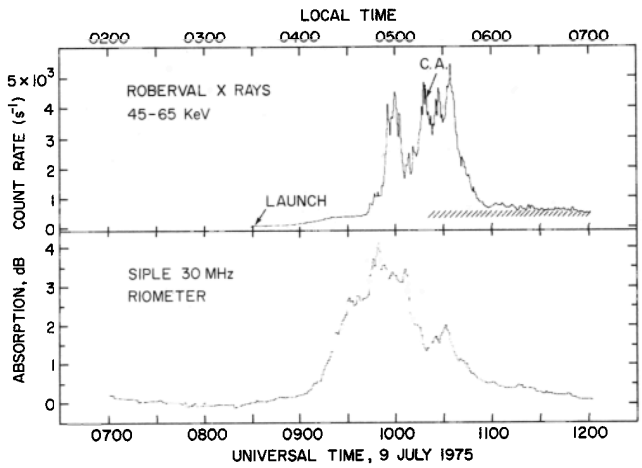

Fig. 10. Substorm electron precipitation data, July 9, 1975, same format as Figure 4. The balloon was launched at 0828 UT and ascended into a precipitation event in progress. It achieved a stable ceiling altitude of 6 g cm^{-2} at 1020 UT.

travel times obtained from the conjugate riser elements. Travel times this small definitely indicate wave propagation outside the plasmapause. Using the diffusive equilibrium (DE) model of field line electron density distribution [*Angerami and Thomas,* 1966; *Park,* 1972] for trial values of 0.7- and 0.8-s travel time we obtain $N = 35$ and 50 cm^{-3}, respectively. These calculations include an estimate of the ionospheric dispersion based on topside electron density profiles published by *Nelms* [1966].

Interpretation and Discussion

The above analysis has shown that the most significant correlation was found between the wave observations in one hemisphere and the particle-related observations near the conjugate point in the opposite hemisphere. Cyclotron resonance interactions between whistler-mode waves and energetic electrons counterstreaming along the geomagnetic field, can cause this result, as will be shown. In both events the chorus generation region and electron-scattering region may have been separated, as shown in Figure 15. The actual wave growth may have involved transfer of kinetic energy from electrons of lower energy (<30 keV) and larger pitch angle (~30°) than those constituting the microbursts.

Model of the Interaction—July 15, 1975

The July 15 observations can be placed in the framework of the schematic model shown in Figure 15. Because the wave observations showed no evidence of echoing emissions, the 2- to 4-kHz risers at Roberval and Siple must have been caused by separate interactions denoted in Figure 1 by B and A, respectively. The interactions probably occurred in a region limited to within 20° of the equatorial plane, for reasons to be discussed below. Interactions A and B were not independent. When conditions were favorable for wave growth in one direction, they were also favorable for the opposite direction too, as indicated by the VLF observations. However, as we noted with regard to Figure 6, the number of prominent risers at Siple exceeded the number at Roberval. This dissimilarity suggests that the factors which may control or contribute to the interaction, such as external stimuli or differences in the electron distribution functions with pitch angle and/or energy, favored interaction A in preference to B in this event. Regarding external stimuli, the Roberval environment has both power line harmonic radiation and sferics (see Figure 11) that can enter the magnetosphere and trigger risers. (These sources are absent at Siple.) However, these triggering sources were not apparently related to the risers in the records for this event. Note that the few risers recorded at Roberval in the same time interval should be associated with electron microbursts precipitated at Siple for which no data are available.

In the X ray/VLF correlation event discussed by *Rosenberg et al.* [1971] and *Foster and Rosenberg* [1976], both the X ray bursts and the correlated risers ($1.5 \leq f \leq 3.8$ kHz, many triggered by whistlers) were measured at Siple. Weaker discrete emissions recorded in the same frequency range at Roberval exhibited no identifiable correlations. That event was another example of interaction A, but one that required a portion of the electrons directed towards Roberval to mirror above the ionosphere and be precipitated at Siple. As was noted in those papers, this requirement was consistent with the conjugate asymmetry in the mirror heights of the Siple and Roberval loss cones.

Near-Equatorial Origin Outside the Plasmasphere

Applying the analysis procedure of *Rosenberg et al.* [1971] and *Foster and Rosenberg* [1976] to the July 15 data, we now show that the energy-frequency relationship of the bursts and the difference of propagation times for the resonant waves and

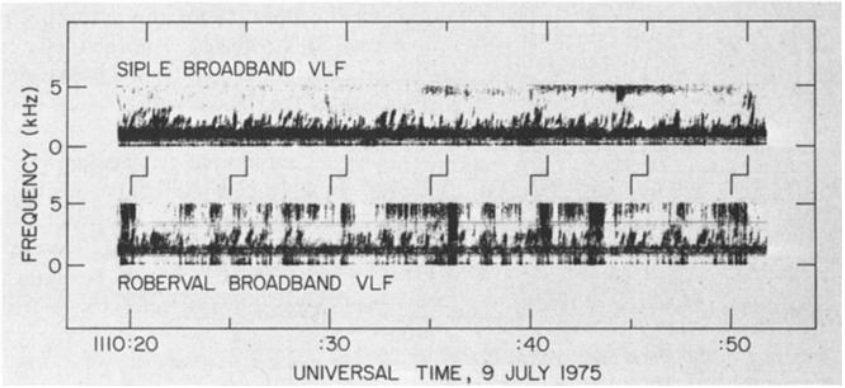

Fig. 11. Siple and Roberval 0–5-kHz VLF spectra. Data are aligned with respect to correlated 2–3.5-kHz chorus riser bursts. Bursts occur first at Siple in this interval. The 0.85-s time offset is indicated by bent lines. (Frequencies below 2 kHz at Roberval are suppressed by a rolloff filter.)

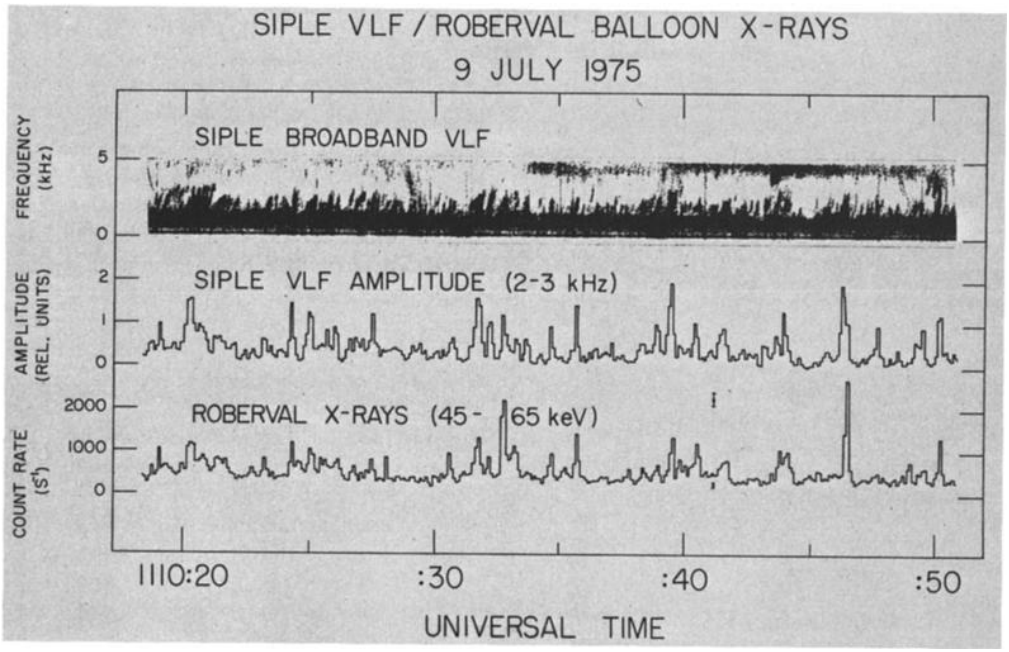

Fig. 12. A 30-s data segment showing simultaneous VLF chorus emissions at Siple and X ray microbursts at Roberval. (Top) 0–5-kHz VLF spectrum; (middle) 2–3-kHz relative amplitude, 0.1-s averages; (bottom) 45–65-keV X ray count rate, 0.1-s averages.

electrons also imply a cyclotron resonance interaction at high altitude on the field line. The rising *df/dt* characteristic of the VLF emissions indicates that the wave growth took place near to, but on the downstream side of, the equatorial plane [*Helliwell*, 1967]. In our analysis we allow the electron scattering to take place on the field line at latitudes that can be well removed from the wave growth region, as suggested by a related correlation found between VLF wave bursts and λ 427.8-nm light bursts [*Helliwell et al.*, 1980]. We have made extensive use of a computer program that models the various physical processes involved and combines them consistently. The program solves the relativistic Doppler-shifted cyclotron resonance equation

$$k_{\parallel} v_{\parallel} = \omega - |\Omega/\gamma| \quad (1)$$

(where $k_{\parallel}$ is the parallel component of the wave number vector, $v_{\parallel}$ is the parallel component of the electron velocity, ω ($=2\pi f$) is the wave frequency, Ω is the electron gyrofrequency, and $\gamma = (1 - v^2/c^2)^{-1/2}$, and then calculates the travel times of the interacting electrons and ducted waves to their respective conjugate points. Input parameters to the program are the interaction (starting) latitude and frequency, a magnetic field model, and the field-line electron density distribution. A dipole magnetic field model was used, since it was found that more accurate (but time consuming) field models do not change calculated travel times by more than a few milliseconds. This program has been found to accurately reproduce the wave group travel time calculations of *Park* [1972]. However, it does not make any allowance for a possibly nonnegligible duration of the scattering process itself. Further discussion is deferred until the treatment of the July 9 event. (This effect must be calculated separately. For the July 15 observations the same conclusions are drawn whether or not this effect is included.)

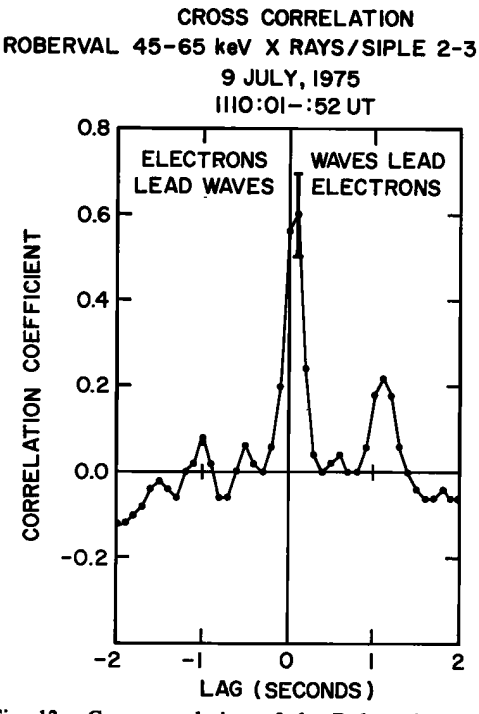

Fig. 13. Cross-correlation of the Roberval 45–65-keV X ray counting rate with the Siple 2–3-kHz VLF signal intensity, 1110 UT July 9, 1975. As on July 15, the most significant peak is a positive correlation, with the X rays delayed by approximately 0.1 s relative to the VLF intensity. The error bar indicates ± 1 standard deviation.

The measured time delay Δt between the reception of VLF risers at Siple and microburst precipitation at Roberval was $0.01 \leq \Delta t \leq 0.13$ s. Travel-time calculations with this program were carried out by using the DE electron density distribution, assuming equatorial electron densities from 4 to 50 cm^{-3}. In Figure 16 are shown selected results for $N_e = 8$, 16, 24, and 32 cm^{-3}. The curves are parametric in wave frequency. Each curve shows the latitude along the $L = 4.1$ field line at which waves of the indicated frequency are resonant with counterstreaming electrons of a particular energy. The horizontal axis displays approximately the range of electron energies produc-

ing the observed X ray microbursts. (An equatorial pitch angle of 4° was assumed for the electrons. This places them just inside the Roberval loss cone.) Only those portions of the curves are plotted for which the calculated arrival time difference ($T_e - T_w$) is between the observed limits 0.01 to 0.13 s. Without this constraint the curves would be symmetric about zero latitude. The steep increase in electron gyrofrequency at field line locations progressively further from the equatorial plane is the cause for the strong dependence of resonant energy on latitude.

Two principal ways in which these calculated results depend on equatorial electron density enable us to place limits on the range of densities that could have been present during the event. First, as the model density is lowered the interaction energy at a given frequency becomes higher. This can

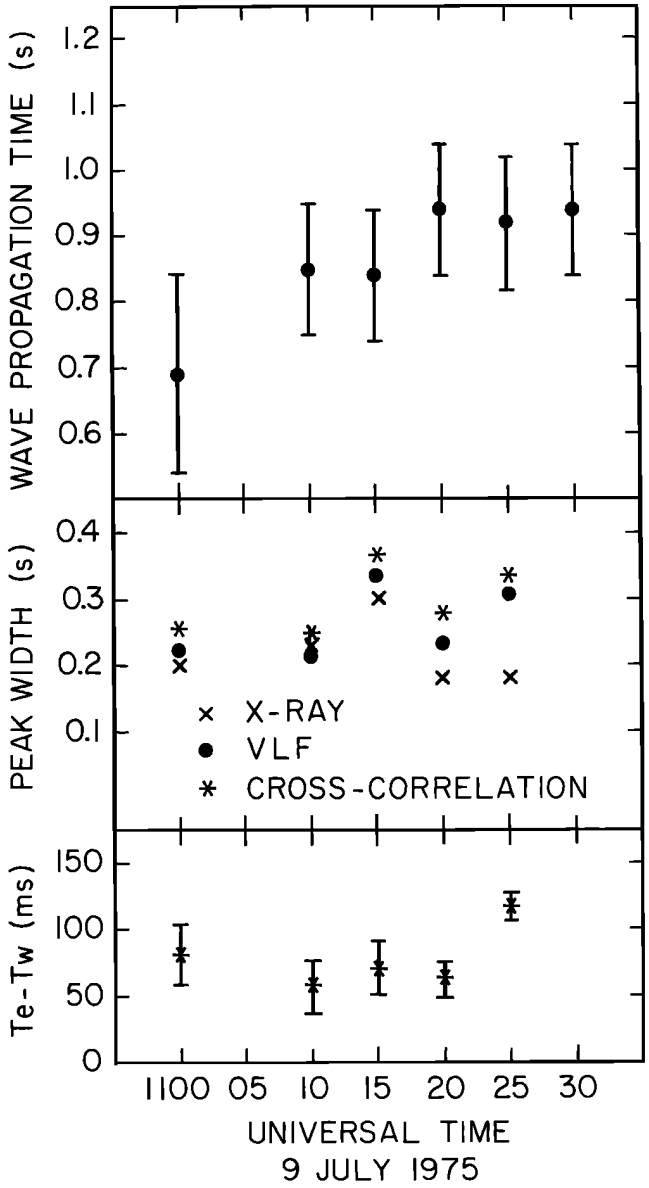

Fig. 14. (Top) Measured whistler-mode propagation time, Siple-Roberval, 2–3.5 kHz; (middle) peak widths (FWHM), X ray/VLF cross correlation and X ray and VLF autocorrelations; and (bottom) electron-wave travel time difference, given by the centroid of the cross-correlation peak. Error bars indicate (top) estimated error in using an overlay technique to correlate VLF data, and (bottom) ± 1 standard error of the mean.

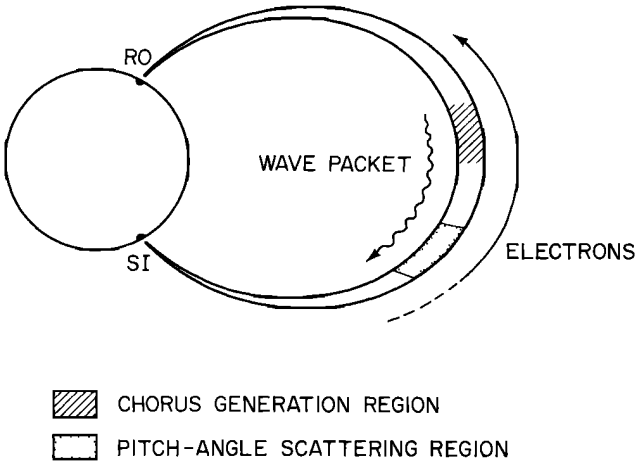

Fig. 15. Schematic model of the wave-particle interaction processes operating on July 9 on the $L = 4.1$ field line. (Also applicable, with somewhat different latitudes, to July 15.) Chorus riser elements are generated downstream (0°–9° N) of the equator, propagate toward Siple, and scatter electrons in the upstream (10°–20°-S) region. The scattered electrons produce bremsstrahlung X rays in the atmosphere over Roberval.

be seen in Figure 16, considering for example, waves of 3-kHz frequency that can interact with electrons of energy as low as 56 keV, if $N_e = 16$ cm^{-3}, but can interact only with electrons of energy above 160 keV if N_e is 4 cm^{-3}. Only if N_e were equal to 8 cm^{-3} or greater could the full observed range of wave frequencies interact with electrons in the energy range that produced the bremsstrahlung X rays. On the other hand, as the electron density is raised, waves of a given frequency become slower and slower. The time constraint on ($T_e - T_w$) could only be satisfied at latitudes further and further removed from the near-equatorial region believed to be the source of VLF chorus. In Figure 16 it can be seen that for $N_e = 32$ cm^{-3} the full range of observed wave frequencies could resonate only at latitudes further than 14° from the equator. This restriction becomes important for $N_e \geq 50$ cm^{-3}. We conclude that equatorial densities in the range $\cong$8–50 cm^{-3} satisfy the interaction and propagation data. These are densities typically found outside the plasmasphere [*Angerami and Carpenter*, 1966].

Information on the location of the plasmapause and the equatorial plasma density at $L = 4.1$ has been obtained from Isis 2 satellite data and from whistlers appearing in the Siple VLF recordings. Figure 17 summarizes this information. The heavy arrows give the estimated positions of the equatorward edge of the light ion trough (LIT) for the two satellite passes that bracket the event in space and time (J. C. Foster, personal communication, 1977). Corresponding changes in the lower hybrid resonance (LHR) noise were also measured on the satellite at these locations. Although this data does not directly provide density information, *Foster et al.* [1978] have shown that the equatorial plasmapause can lie a few degrees poleward of the equatorward edge of the light ion trough in the morning sector.

Equatorial densities determined from whistlers are shown in Figure 17 at two times: 1325 and 1420 UT. The whistler at 1420 UT provided the estimate of ~14 cm^{-3} at $L = 4.4$. The parallelogram-shaped region associated with this point is a measure of the uncertainties in scaling the VLF spectrogram. *Angerami and Carpenter* [1966] have found empirically that the equatorial distribution of density outside the plasmapause often varies as L^{-4}. Extrapolating inward from $L = 4.4$, using

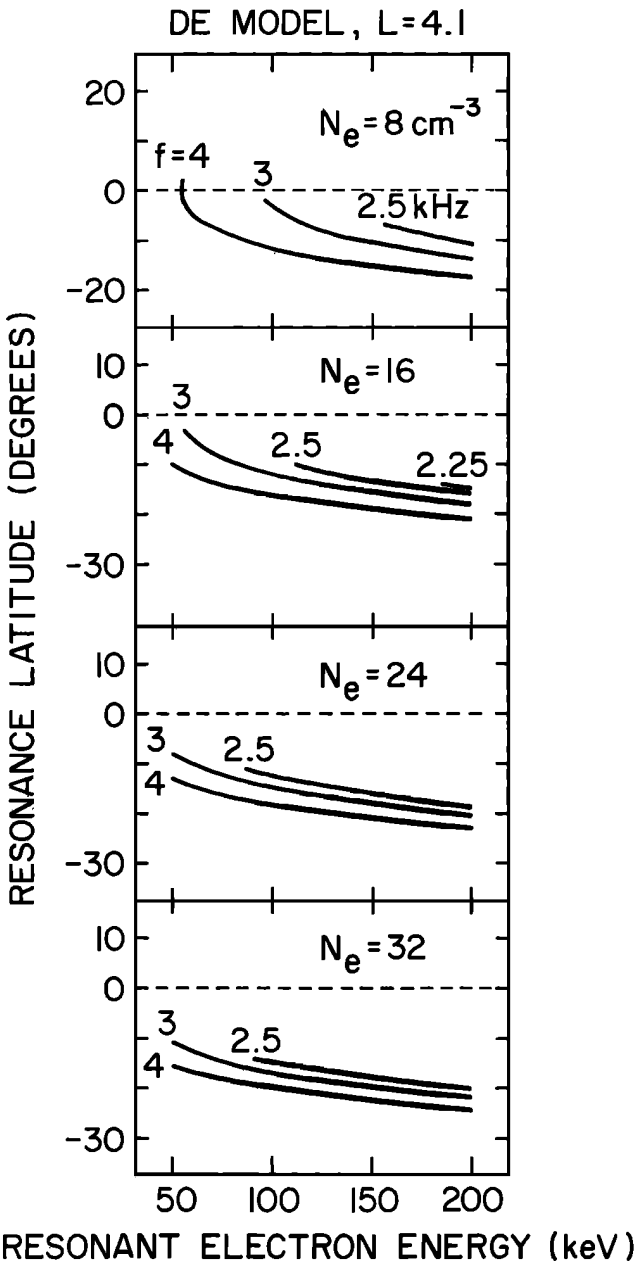

Fig. 16. Calculated resonance latitude dependence on electron energy and equatorial electron density N_e. The diffusive equilibrium (DE) electron density distribution is used. The curves are parametric in wave frequency. Only those portions of the curves are plotted for which $0.01 \text{ s} \leq (T_e - T_w) \leq 0.13$ s. Positive latitudes are northward of the equatorial plane.

$N_e \propto L^{-4}$, we estimate that N_e = 15–25 cm^{-3} at L = 4.1, in agreement with the X ray/VLF result. The high density values inside L = 3.4 appear to be near the outer limits of the equatorial plasmasphere at the times of the observations, in approximate agreement with the position inferred from the satellite measurements.

Because a 'collisionless' field-line electron density distribution has been thought to have some theoretical justification [*Angerami*, 1966] it was used to interpret the high-latitude whistler at 1420 UT (giving N_e = 3.5 cm^{-3} at L = 4.7) and was employed in several simulation runs in our computer program using the lower equatorial densities obtained by extrapolating the 1420 UT whistler. The collisionless distribution has in general a much steeper altitude dependence than the DE distribution. Because of its similarity to the distribution $N \propto R^{-4}$, we shall use the description 'R^{-4}' in what follows. In Figure 18 are shown, in the same format as Figure 16, results of the calculations that use the R^{-4} distribution. Only those portions of the curves satisfying the arrival time difference observation are plotted. In contrast to the calculations that use the DE distribution, these calculations cannot account for the observations. For no energy or density could the full observed range of wave frequencies (2–3.5 kHz) interact with resonant electrons at any latitude along the field line. Only for improbably small electron densities (<4 cm^{-3}) could waves of less than 3 kHz resonate with 50–200-keV electrons, which are the source of the X rays. Consequently, the R^{-4} field line density distribution must be rejected.

Although most chorus is attributed to wave growth in near-equatorial cyclotron resonance interactions, details of the relevant mechanism or instability remain in doubt. We have pointed out (Figure 6) the tendency of the Siple risers on July 15 to shift initially to a higher frequency and then to a lower frequency during the sequence. Presumably, this frequency shift is related to a specific feature of the mechanism or instability controlling wave growth. The present data set alone cannot resolve questions of such detail, but the effect may result from changes in the energetic particle flux or in the anisotropy of the distribution function [*Helliwell*, 1967; *Burton and Holzer*, 1974; *Maeda*, 1976; *Anderson and Maeda*, 1977]. For cyclotron resonance, whistler-mode waves are unstable to wave growth if $A > 1/(f_g/f - 1)$, where A is a measure of resonant electron pitch angle anisotropy and f_g is the local electron gyrofrequency [*Kennel and Petschek*, 1966]. As the anisotropy increases (decreases) the peak of emission shifts to higher (lower) frequency. Thus the observed frequency shifts could be accounted for by a similar systematic trend of the anisotopy. Wave growth would depend on the anisotropy factor and on the fraction of electrons that are resonant.

Model of the Interaction—July 9, 1975

The same basic mechanism of wave-particle interaction that was shown above to account for the July 15 observations also provides a framework for the understanding of the July 9 correlations. In this case the higher statistical significance of the results and the availability of electron density information for the Roberval-Siple field line lead naturally to a different method of analysis. Computer calculations were performed that modeled the wave-particle interaction and subsequent travel of the scattered electrons and ducted waves to conjugate ionospheres. In these calculations, equatorial electron densities were selected from a relatively narrow range consistent with the wave travel time observations. Figure 19 shows (solid curves) the calculated arrival time difference for a wave frequency of 2.5 kHz and equatorial electron densities of N_e = 35 and 50 cm^{-3}. Also shown, for comparison, is the calculated arrival time difference for an R^{-4} electron density distribution that gives the same wave propagation time as the N_e = 50 cm^{-3} DE distribution. Resonant electron energies are not shown, but only those portions of the curves are plotted for which the resonant energy is less than 200 keV. The cross-hatched strip at the top represents the range of travel time differences, $0.036 \text{ s} \leq (T_e - T_w) \leq 0.128$ s, observed between 1100 and 1125 UT (Figure 14).

It is immediately evident in Figure 19 that a gap is present between even the largest calculated value of $(T_e - T_w$, and the range of observed arrival time differences. Calculations performed for other wave frequencies in the chorus band also

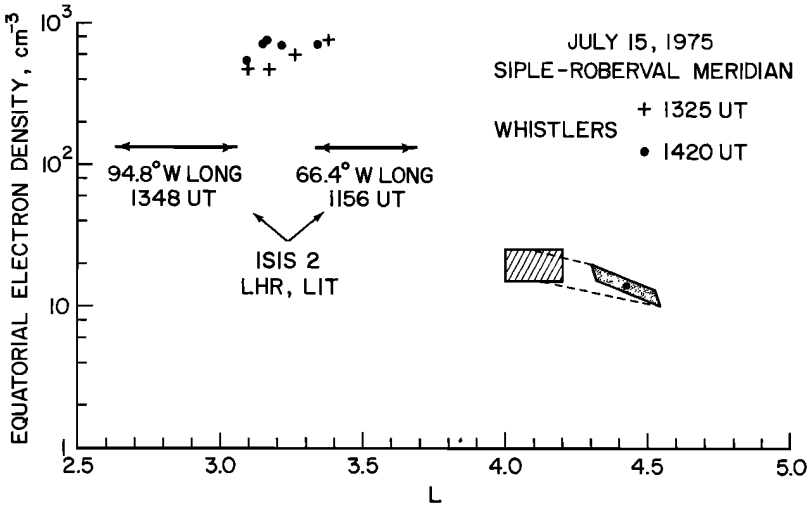

Fig. 17. Estimated plasmapause location and equatorial electron densities determined from two data sources: (1) Whistler traces appearing on the Siple VLF records at the times indicated predict the high plasmaspheric densities inside $L = 3.4$ and the low estimate of ~14 cm^{-3} centered at $L = 4.4$ outside the plasmasphere. The L^{-4} model is used to extrapolate (dashed lines) the $L = 4.4$ estimate, with measurement uncertainty, to the Siple vicinity ($L = 4.1 \pm 0.1$), giving a density N_e of 15–25 cm^{-3}. (2) The heavy arrows show the locations of the equatorward edge of the light ion trough (LIT) and corresponding signatures in lower hybrid resonance (LHR) noise data for two satellite passes that bracket the event in space and time (Roberval is located at 72.25°W). This data does not directly provide information, but according to *Foster et al.* [1978], the equatorial plasmapause projection on the ionosphere lies several degrees poleward of the equatorward edge of the LIT in the morning sector during disturbed conditions.

have this characteristic gap. Moderate relaxation of the energy or electron density constraints cannot bridge the gap because of a focusing effect peculiar to the upstream (southern) latitudes. The focusing in arrival time basically results from the faster motion of electrons resonant at higher upstream latitudes, which allows them to partially overtake less energetic electrons resonant closer to the equator.

We interpret the existence of this time gap as evidence that the duration of the electron scattering process itself was not negligible in this event. The finite pitch-angle scattering time of the resonant electrons taken in the aggregate is what determines the mean arrival time of the observed electron bursts. The scattering process can be understood as follows: Each energetic electron, on encountering a whistler-mode wave packet with which it is resonant, may be scattered into the loss cone at a time S_i after passing the leading edge of the wave packet. S_i depends on the phase, pitch angle, and precise energy of the resonant electron. For each electron scattered into the loss cone, the quantity S_i is less than S_p, where S_p is the duration of the wave packet in the frame of reference of the moving electron. The centroid of the observed burst of precipitation then is delayed by $\langle S_i \rangle$, the mean scattering time, which can take any value from 0 to S_p. In allowing for the effective delay resulting from $\langle S_i \rangle$ being nonzero in a particular case, it is necessary to know both the rest-frame wave packet duration and the transformation that converts this quantity to the duration in the resonant electron frame. For the former we use an estimate based on the VLF autocorrelation width, realizing that actual chorus riser elements can be a factor of ~2 briefer or longer. If T is the wave packet duration in the rest frame, it can be shown that the transformation that converts T into S, the wave packet duration in the resonant electron frame, is

$$\mathbf{S} = \left(\frac{v_g}{v_g + v_\parallel}\right)\mathbf{T} \qquad (2)$$

where v_g is the wave group velocity, and $v_\parallel$ is the parallel component of the particle velocity. In Figure 20 is plotted the ratio S/T as a function of interaction latitude for the wave frequency 2.5 kHz. Each curve represents one of the electron density distributions used in Figure 19. The dependence on latitude is similar for all the distributions. The ratio S/T is largest at the equator, where v_g has a broad maximum, and $v_\parallel$ is a minimum. Most of the variation within ± 15° of the equator is due to the latitude dependence of $v_\parallel$. Taking as a trial estimate T = 0.25 s (a typical VLF autocorrelation peak width), and the calculated S/T ratios, we have adjusted each of the $(T_e - T_w)$ curves in Figure 19 by displacing it an amount S corresponding to the maximum possible delay caused by nonzero scattering time. The resulting curves are shown dashed.

When the effect of nonzero scattering time is estimated and included in the arrival time difference calculations for the DE distribution as described above, the calculations are just brought into agreement with the measured values at latitudes 10°-20°S. Nearly the maximum possible delay is required. No agreement is obtained with the R^{-4} electron density distribution calculations. The arrival time differences derived from the DE distribution more nearly agree (Figure 19) with the observations than differences derived from the R^{-4} distribution. One might infer that distributions having even less increase with latitude than the DE distribution (or no increase) could be found that would produce even closer agreement. This is correct, but no distribution without an equatorial density maximum can match the range of observations without a significant scattering time contribution, such as those shown in Figure 19. Such peaked density distributions lack the simplicity of the DE or R^{-4} distributions, but may be present under transient conditions [*Banks et al.*, 1971; *Rösler*, 1975; *Titheridge*, 1976]. However, as Banks et al. have also shown, nonequilibrium distributions quickly (in a few hours at $L \approx 4$) revert to near-equilibrium distributions, even when the densities are far below plasmaspheric levels. This was the most likely situation during both the July 9 and July 15 events.

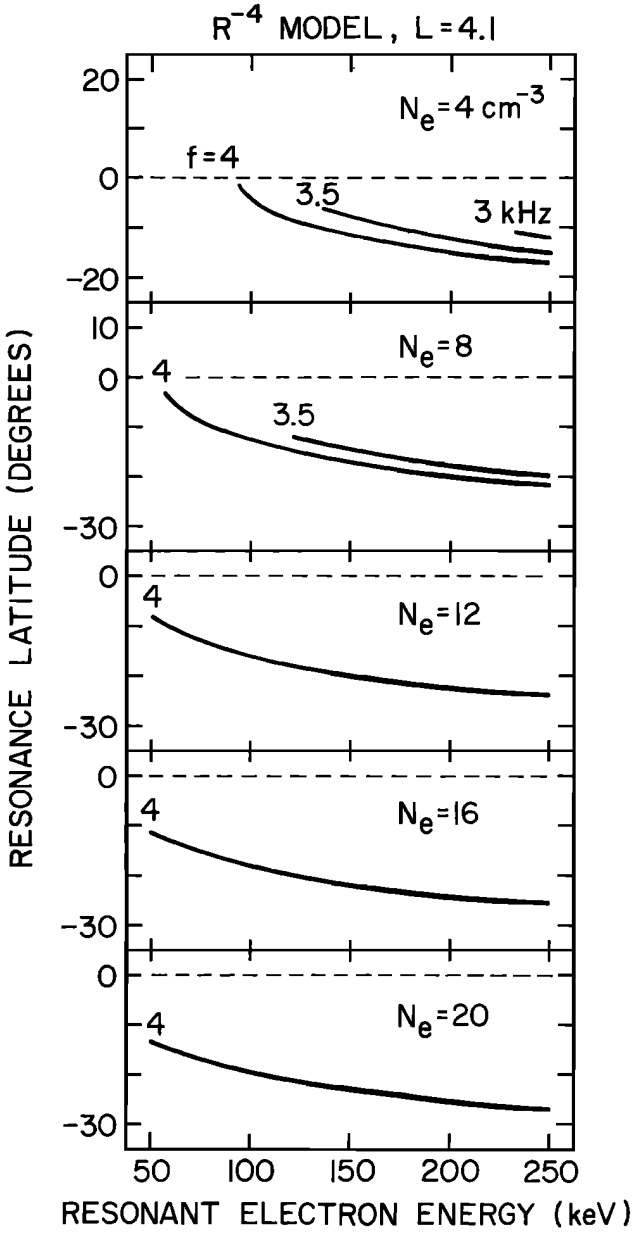

Fig. 18. Calculated resonance latitude dependence on electron energy and equatorial electron density N_e. (The format is the same as Figure 16, except that the R^{-4} electron density distribution was used.)

In Figure 15 are shown schematically the processes we believe were operating on July 9. A magnetic flux tube at $L = 4.1$ is indicated to scale (the thickness is exaggerated for clarity). A chorus generation region is shown downstream of the equatorial plane and bounded by it. The size of this region cannot be determined from our data, but we have used the measured df/dt values of the riser elements to compute a latitudinal upper limit (9°N) on the location of the high latitude boundary, following *Helliwell* [1967, equation (15)]. In any case the positive slope df/dt of the riser elements indicates a downstream chorus generation region. Also shown is our estimate of the location of the pitch-angle scattering region at latitudes 10°–20°S. Resonant electrons scattered at these latitudes have energies 40–200 keV. It is interesting to note that it is these latitudes at which the 'focusing effect' mentioned above occurs. The 'focusing effect' may play a part in shaping the microbursts, in regard to rise time and width, as suggested by *Helliwell et al.* [1980].

We suggest that on July 9 the chorus generation region and electron pitch-angle scattering region were separated, as shown in Figure 15. The waves propagated southward, resonating with progressively higher energy electrons, finally, at 10°–20°S, scattering electrons of sufficiently high energy to produce the observed bremsstrahlung X rays. It is tempting to speculate that the pitch-angle scattering proceeded with more or less equal vigor all along the field line from the point of origin of the waves, but our data are not sufficient to address this question. Evidence for scattering by triggered emissions in the region upstream of the interaction region has been found in the so-called 'quiet band' effect [*Raghuram et al.*, 1977].

Summary and Conclusions

Conjugate observations of bremsstrahlung X rays and discrete VLF emissions at $L = 4.1$ have been presented. The observations and subsequent analysis have led to the following conclusions.

1. A detailed correlation in two events was found between electron microbursts ($50 \lesssim E \lesssim 200$ keV) and chorus elements of rising frequency ($2 \lesssim f \lesssim 4$ kHz) observed at ionospheric conjugate points of the geomagnetic field.

2. The electron microbursts in one hemisphere (Roberval, Canada) were observed to lag the associated risers in the opposite hemisphere (Siple Station, Antarctica) in one event by 0.07 ± 0.06 s and in another event by $.08 \pm .04$ s.

3. The observed relationship between electron energy and wave frequency and the measured time delay are consistent with generation of the bursts by cyclotron resonance interactions near (within 20° of) the equatorial plane, followed by propagation of the resonant (scattered) electrons and waves along the geomagnetic field to the conjugate ionospheres. In one event there is evidence that the process of pitch-angle scattering itself may require a time (0.06–0.08 s) nearly equal to the full duration of the chorus riser elements encountered by the resonant electrons.

4. In one event a value of ~8 to 50 cm^{-3} for the equatorial plasma density at $L \approx 4.1$ is deduced from the microburst-

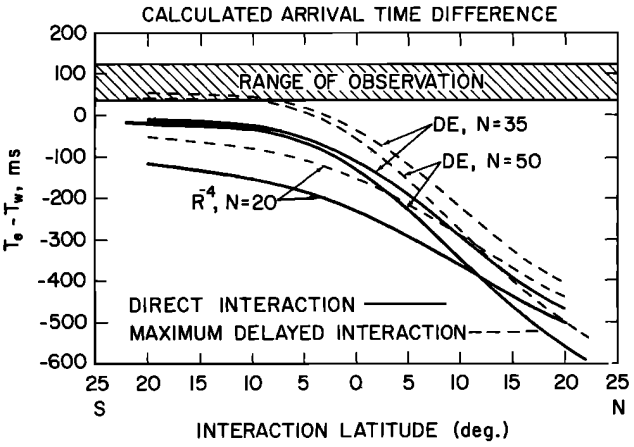

Fig. 19. Arrival time difference ($T_e - T_w$) calculated as a function of resonant latitude for wave frequency 2.5 kHz. Two DE electron density distributions and an R^{-4} distribution are shown (solid curves). The dashed curves show the effect of the maximum delay resulting from a nonzero scattering time (see text). The hatched area shows the range of electron-wave arrival time differences measured on July 9, 1975.

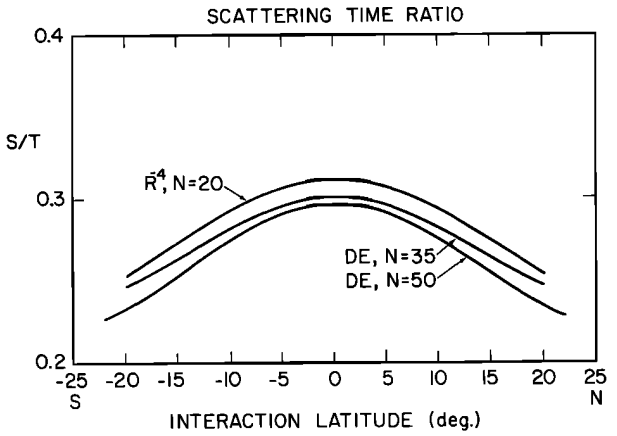

Fig. 20. Scattering time ratio S/T at the wave frequency 2.5 kHz on the L 4.1 field line. S is the wave packet duration in the resonant electron frame, and T is the wave packet duration in the rest frame. Electron density distributions are those used in Figure 19. See text for details.

chorus data, indicating that the interaction region is outside the plasmasphere. This estimate is in agreement with a whistler density estimate and with the position of the plasmapause as determined from whistlers and from signatures in Isis 2 light-ion and lower-hybrid-resonance noise data. In the other event the propagation time of the observed chorus also indicated that the interaction was outside the plasmasphere (N_e 35–50 cm^{-3}). In both events the observations could be accounted for only in terms of a diffusive-equilibrium distribution of electron density along the field line. The 'collisionless' (or R^{-4}) model of electron density was not in accord with the observations.

In conclusion, the observations described bear on the question of microburst source location. Our results for $L \cong 4$ together with the few others available at higher latitudes (cited in the introduction) suggest that microburst generation regions are located near the equator on subauroral field lines but may extend to higher magnetic latitudes along the field line for larger L values. A similar L dependence of the location and extent of dayside chorus generation regions has been reported by *Tsurutani and Smith* [1977].

Acknowledgments. Ttis research was a collaborative effort by several groups who used the facilities at Roberval, Canada, and Siple Station, Antarctica, to study wave-particle interactions in the magnetosphere. The balloon flights carried out by the University of Maryland were sponsored by the Division of Polar Programs of the National Science Foundation under grant DPP 74-01704 and by the Office of Naval Research under contract N00014-67-A-0239-0033. Analysis of the data has continued under NSF grants DPP 76-82041 and DPP 80-12901. Field support during launch operations was provided by S. Bergersen, E. Bering, C. Gibson, and C. Liles. We thank J. Katsufrakis of Stanford University for his overall coordination of Siple and Roberval activities. The research at Stanford was supported by the Division of Polar Programs of the National Science Foundation under grant DPP76-82646 and by the Atmospheric Sciences Section of the NSF under grant ATM75-07707. D. Detrick of the University of Maryland and A. Gault and R. Streeter of the Information Processing Division of the Goddard Space Flight Center provided valuable assistance with X ray data processing. Additional support was obtained from the Computer Science Center of the University of Maryland. We thank L. J. Lanzerotti of Bell Laboratories for providing a magnetometer for use at the Roberval launch site, and for Lac Rebours magnetometer data. The College magnetometer data were obtained from WDC-A for Solar Terrestrial Physics (Geomagnetism). Acquisition of the Siple riometer data involved the cooperation of H. Chivers of the University of California, San Diego, and L. J. Lanzerotti. J. C. Foster of Utah State University obtained the Isis 2 light ion data and provided useful comments. One of the authors (T. J. R.) acknowledges the support of the Royal Norwegian Council for Scientific and Industrial Research and the hospitality of The Norwegian Institute of Cosmic Physics, University of Oslo, during the initial work on this paper.

The Editor thanks J. C. Foster and G. K. Parks for their assistance in evaluating this paper.

REFERENCES

Anderson, R. R., and K. Maeda, VLF emissions associated with enhanced magnetospheric electrons, *J. Geophys. Res., 82,* 135, 1977.

Anderson, K. A., and D. W. Milton, Balloon observations of X rays in the auroral zone, 3, High time resolution studies, *J. Geophys. Res., 69,* 4457, 1964.

Angerami, J. J., and J. O. Thomas, Studies of planetary atmospheres, 1, The distribution of electrons and ions in the earth's exosphere, *J. Geophys. Res., 69,* 4537, 1966.

Angerami, J. J., A whistler study of the distribution of thermal electrons in the magnetosphere, *Tech. Rep. 3412-7,* Stanford Electron. Lab., Stanford Univ., Stanford, Calif., 1966.

Angerami, J. J., and D. L. Carpenter, Whistler studies of the plasmapause in the magnetosphere, 2, Electron density and total tube content near the knee in magnetospheric ionization, *J. Geophys. Res., 71,* 711, 1966.

Banks, P. M., A. F. Nagy, and W. I. Axford, Dynamical behavior of thermal protons in the mid-latitude ionosphere and magnetosphere, *Planet. Space Sci., 19,* 1053, 1971.

Barish, F. P., and R. E. Wiley, World contours of conjugate mirror locations, *J. Geophys. Res., 75,* 6342, 1970.

Brice, N. M., An explanation of triggered very low frequency emissions, *J. Geophys. Res., 68,* 4626, 1963.

Burtis, W. J., and R. A. Helliwell, Banded chorus—A new type of VLF radiation observed in the magnetosphere by OGO 1 and OGO 3, *J. Geophys. Res., 74,* 3002, 1969.

Burtis, W. J., and R. A. Helliwell, Magnetospheric chorus: Occurrence patterns and normalized frequency, *Planet. Space. Sci., 24,* 1007, 1976.

Burton, R. K., and R. E. Holzer, The origin and propagation of chorus in the outer magnetosphere, *J. Geophys. Res., 79,* 1014, 1974.

Dowden, R. L., Doppler-shifted cyclotron radiation from electrons: A theory of very low frequency emissions from the exosphere, *J. Geophys. Res., 67,* 1745, 1962.

Dowden, R. L., Electron energy spectrum and structure deduced from analysis of VLF discrete emissions by using the Helliwell criterion, *J. Geophys. Res., 76,* 3034, 1971.

Dunckel, N., and R. A. Helliwell, Whistler-mode emissions on the OGO 1 satellite, *J. Geophys. Res., 74,* 6371, 1969.

Foster, J. C., and T. J. Rosenberg, Electron precipitation and VLF emissions associated with cyclotron resonance interactions near the plasmapause, *J. Geophys. Res., 81,* 2183, 1976.

Foster, J. C., C. G. Park, L. H. Brace, J. R. Burrows, J. H. Hoffman, E. J. Maier, and J. H. Whitteker, Plasmapause signatures in the ionosphere and magnetosphere, *J. Geophys. Res., 83,* 1175, 1978.

Haugstad, B. S., and T. Pytte, Effects of primary electron transit times on power spectra of auroral-zone X ray microbursts, *J. Atmos. Terr. Phys., 39,* 689, 1977.

Helliwell, R. A., *Whistlers and Related Ionospheric Phenomena,* Stanford University Press, Stanford, California, 1965.

Helliwell, R. A., A theory of discrete VLF emissions from the magnetosphere, *J. Geophys. Res., 72,* 4773, 1967.

Helliwell, R. A., Intensity of discrete VLF emissions, in *Particles and Fields in the Magnetosphere,* edited by B. M. McCormack, p. 292, D. Reidel, Hingham, Mass., 1970.

Helliwell, R. A., and T. L. Crystal, A feedback model of cyclotron interaction between whistler mode waves and energetic electrons in the magnetosphere, *J. Geophys. Res., 78,* 7357, 1973.

Helliwell, R. A., S. B. Mende, J. H. Doolittle, W. C. Armstrong, and D. L. Carpenter, Correlations between λ4278 optical emissions and VLF wave events observed at $L \sim 4$ in the Antarctic, *J. Geophys. Res., 85,* 3376, 1980.

Kennel, C. F., and H. E. Petschek, Limit on stably trapped particle fluxes, *J. Geophys. Res., 71,* 1, 1966.

Lampton, M., Daytime observations of energetic auroral-zone electrons, *J. Geophys. Res., 72,* 5817, 1967.

Lanzerotti, L. J., C. G. Maclennan, and C. Evans, Association of ULF

magnetic variations and changes of ionospheric conductivity, *J. Geophys. Res., 83,* 2525, 1978.
Maeda, K., Cyclotron side-band emissions from ring-current electrons, *Planet. Space Sci., 24,* 341, 1976.
Matsumoto, H., and I. Kimura, Linear and nonlinear cyclotron instability and VLF emissions in the magnetosphere, *Planet. Space Sci., 19,* 567, 1971.
Nakano, G. H., W. L. Imhof, and J. B. Reagan, Coherent microburst electron precipitation measured from a satellite, *J. Geomagn. Geoelectr., 30,* 347, 1978.
Nelms, G. L., Seasonal and diurnal variations of the distribution of electron density in the topside of the ionosphere, in *Electron Density Profiles in the Ionosphere and Exosphere,* edited by John Frihagen, John Wiley, New York, 1966.
Nunn, D., A theory of VLF emissions, *Planet. Space Sci., 19,* 1141, 1971.
Nunn, D., A self-consistent theory of triggered VLF emissions, *Planet. Space Sci., 22,* 349, 1974.
Oliven, M. N., and D. A. Gurnett, Microburst phenomena, 3, An association between microbursts and VLF chorus, *J. Geophys. Res., 73,* 2355, 1968.
Oliven, M. N., D. Venkatesan, and K. G. McCracken, Microburst phenomena, 2, Auroral-zone electrons, *J. Geophys. Res., 73,* 2345, 1968.
Park, C. G., Methods of determining electron concentrations in the magnetosphere from nose whistlers, *Tech. Rep. 3454-1,* Stanford Electron. Lab., Stanford Univ., Stanford, Calif., 1972.
Parks, G. K., Auroral zone microbursts, substructures, and a model for microburst precipitation, *Proc. Int. Conf. X-Rays Space* (Cosmic, Sol. Auroral X-Rays), *2,* 849–874, 1975.
Parks, G. K., Microburst precipitation phenomena, *J. Geomagn. Geoelectr., 30,* 327, 1978.
Raghuram, R., T. F. Bell, R. A. Helliwell, and J. P. Katsufrakis, A quiet band produced by VLF transmitter signals in the magnetosphere, *Geophys. Res. Lett., 4,* 199, 1977.
Rosenberg, T. J., R. A. Helliwell, and J. P. Katsufrakis, Electron precipitation associated with discrete very low frequency emissions, *J. Geophys. Res., 76,* 8445, 1971.
Rosenberg, T. J., J. C. Foster, D. L. Matthews, W. R. Sheldon, and J. R. Benbrook, Microburst precipitation at $L \approx 4$, *J. Geophys. Res., 82,* 177, 1977.
Rosenberg, T. J., K. Marthinsen, J. A. Holtet, A. Egeland, and D. L. Carpenter, Evidence of the common origin of electron microbursts and VLF chorus, *J. Geomagn. Geoelectr., 30,* 355, 1978.
Rösler, G., Supersonic plasma flow between high-latitude conjugate ionospheres, *J. Geophys., 41,* 413, 1975.
Siren, J. C., T. J. Rosenberg, D. Detrick, and L. J. Lanzerotti, Conjugate observation of electron microburst groups by bremsstrahlung X ray and riometer techniques, *J. Geophys. Res., 85,* 6760, 1980.
Sudan, R. N., and E. Ott, Theory of triggered VLF emissions, *J. Geophys. Res., 76,* 4463, 1971.
Titheridge, J. E., Plasmapause effects in the topside ionosphere, *J. Geophys. Res., 81,* 3227, 1976.
Tsurutani, B. T., and E. J. Smith, Two types of magnetospheric ELF chorus and their substorm dependences, *J. Geophys. Res., 82,* 5112, 1977.
Zhulin, I. A., J.-P. Treilhou, and J. Gasset, Roentgen bremsstrahlung at subauroral latitudes, *Kosm. Issled., 11,* 441, 1973.

(Received November 20, 1980;
revised March 13, 1981;
accepted March 16, 1981.)